

1 Supplementary information

2 Self-Supervised Denoising for Enhanced Volumetric 3 Reconstruction and Signal Interpretation in 4 Two-photon Microscopy

5 Jie Li^{1,2}, Liangpeng Wei³, and Xin Zhao^{1,2,*}

6 ¹National Key Laboratory of Intelligent Tracking and Forecasting for Infectious Diseases, Engineering Research

7 Center of Trusted Behavior Intelligence, Ministry of Education, Tianjin Key Laboratory of Intelligent Robotic (tikLIR),

8 Institute of Robotics & Automatic Information System (IRAIS), Nankai University, Tianjin 300350, China

9 ²Shenzhen Research Institute of Nankai University, Shenzhen 518083, China.

10 ³School of Biomedical Engineering and Technology, Tianjin Medical University, Tianjin 300070, China.

11 *corresponding author: Xin Zhao (zhaoxin@nankai.edu.cn)

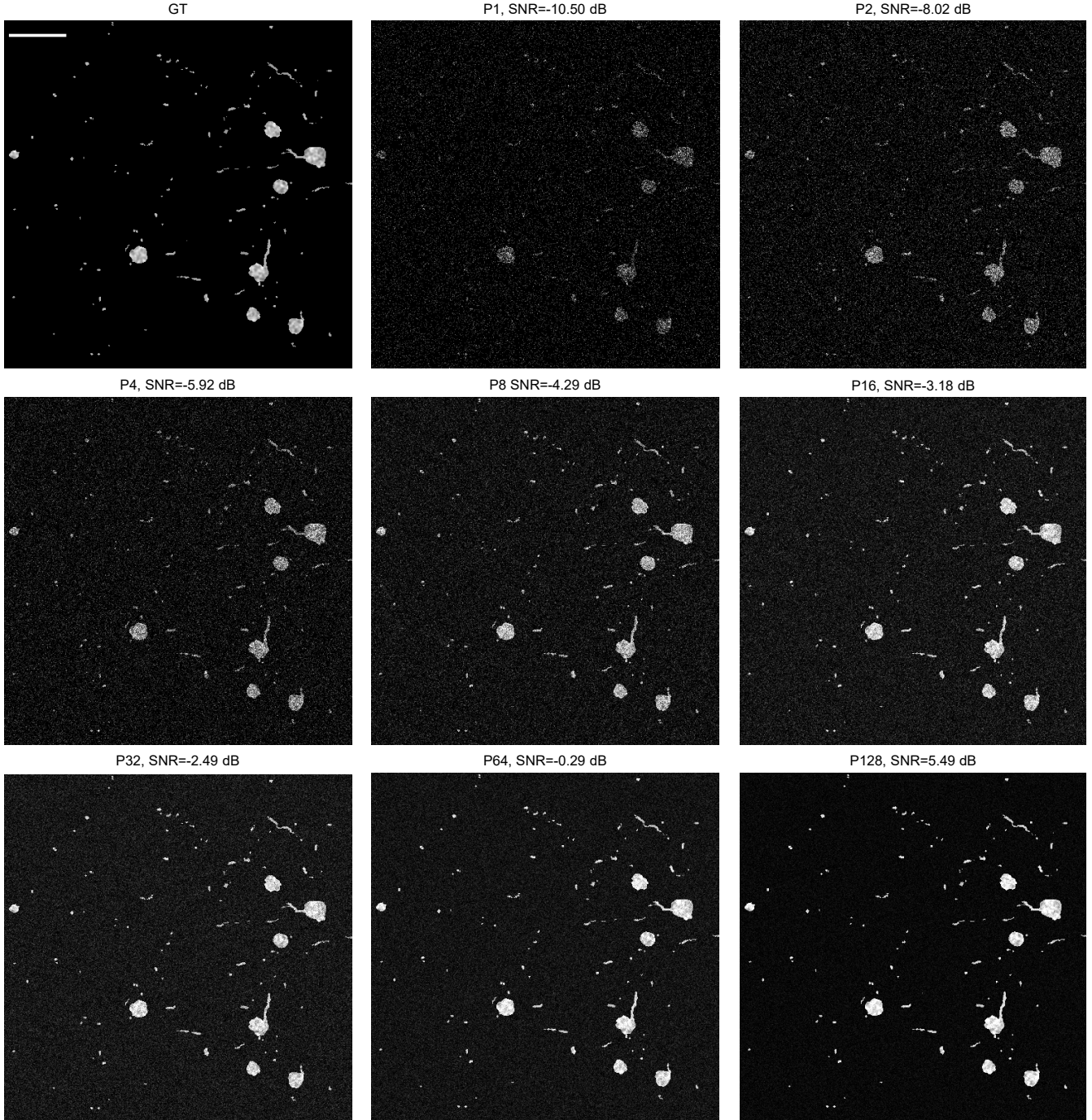
¹² **CONTENTS**

¹³ **Supplementary Figures S1-S16**

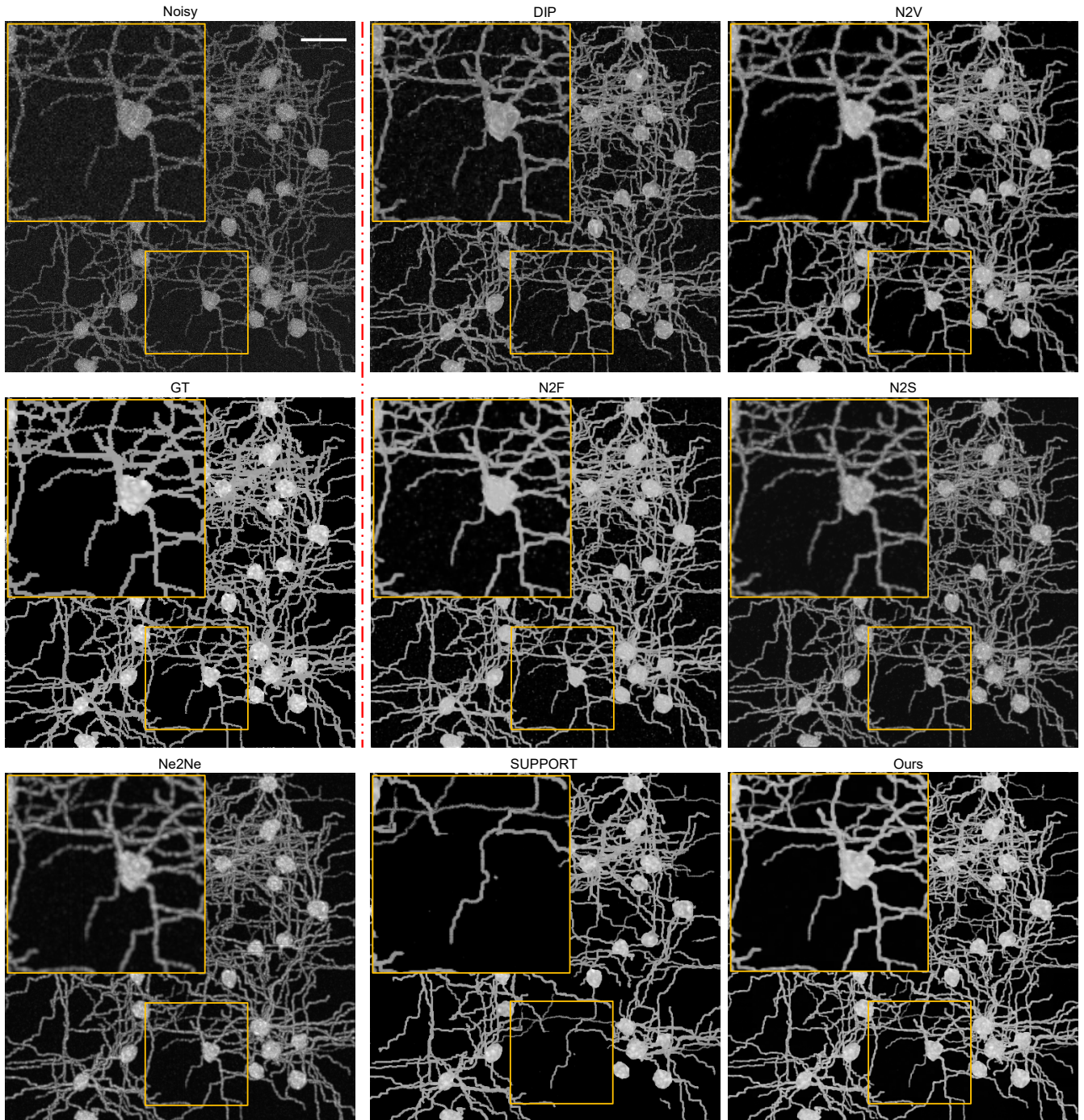
¹⁴ **Supplementary Table S1-S3**

¹⁵ **Supplementary Videos S1-S9**

¹⁶ **Supplementary Figures**

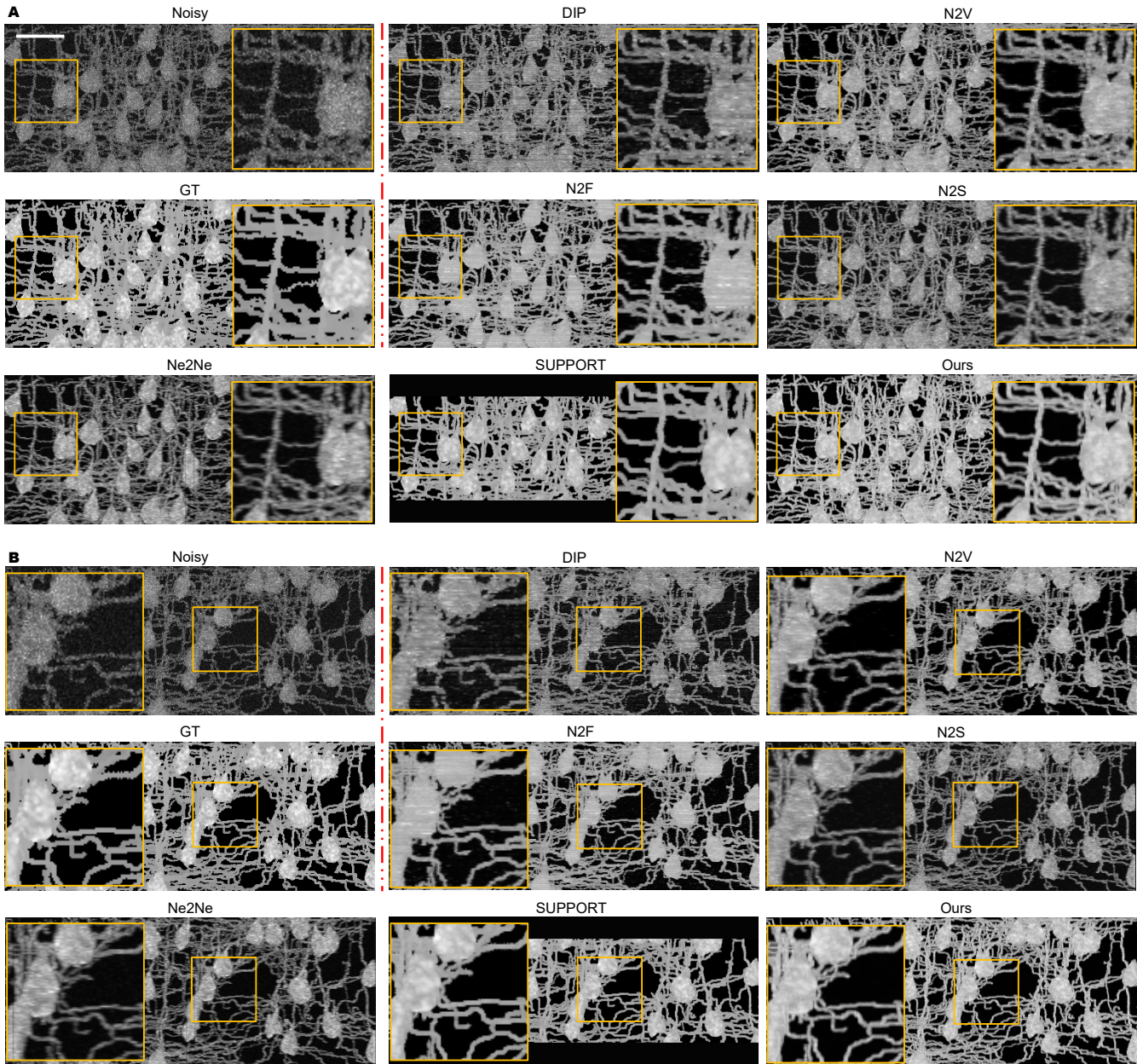


Supplementary Fig. S1. Simulation of structural imaging data. Representative images of different imaging SNRs and corresponding ground truth (GT). Noise-free structural imaging stacks were simulated based on NAOMi¹. Different levels of Mixed Poisson-Gaussian noise were added subsequently. Noise-free images were used as the ground truth for quantitative evaluations of the denoising performance. Scale bar, 50 μm .



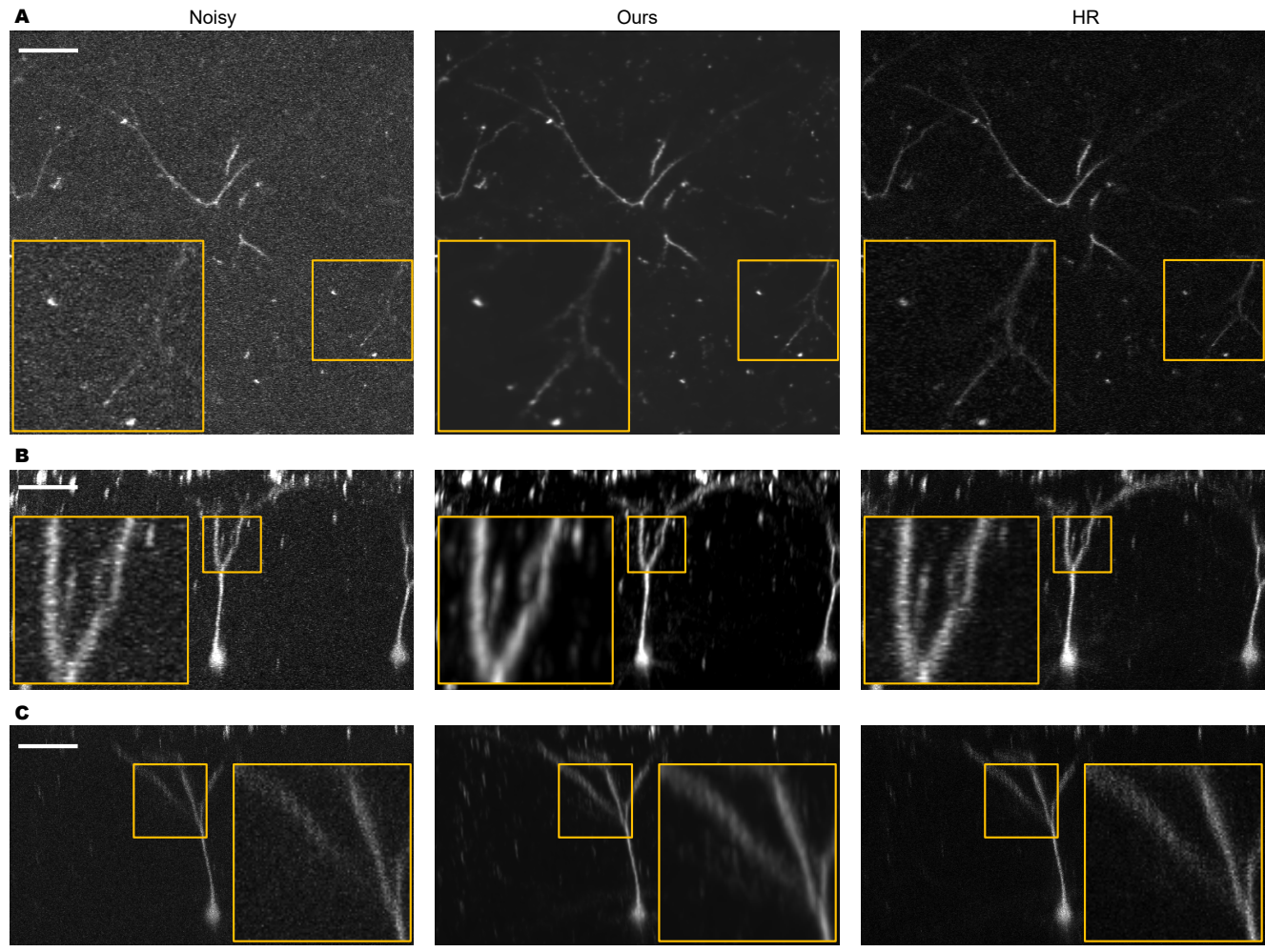
18

Supplementary Fig. S2. Max projection images for method comparison. Max projection images along z axis of the whole volume with $250 \times 250 \times 100 \mu\text{m}^3$ (200 planes, $0.5 \mu\text{m}/\text{pixel}$ in three axes), for comparison of different methods.



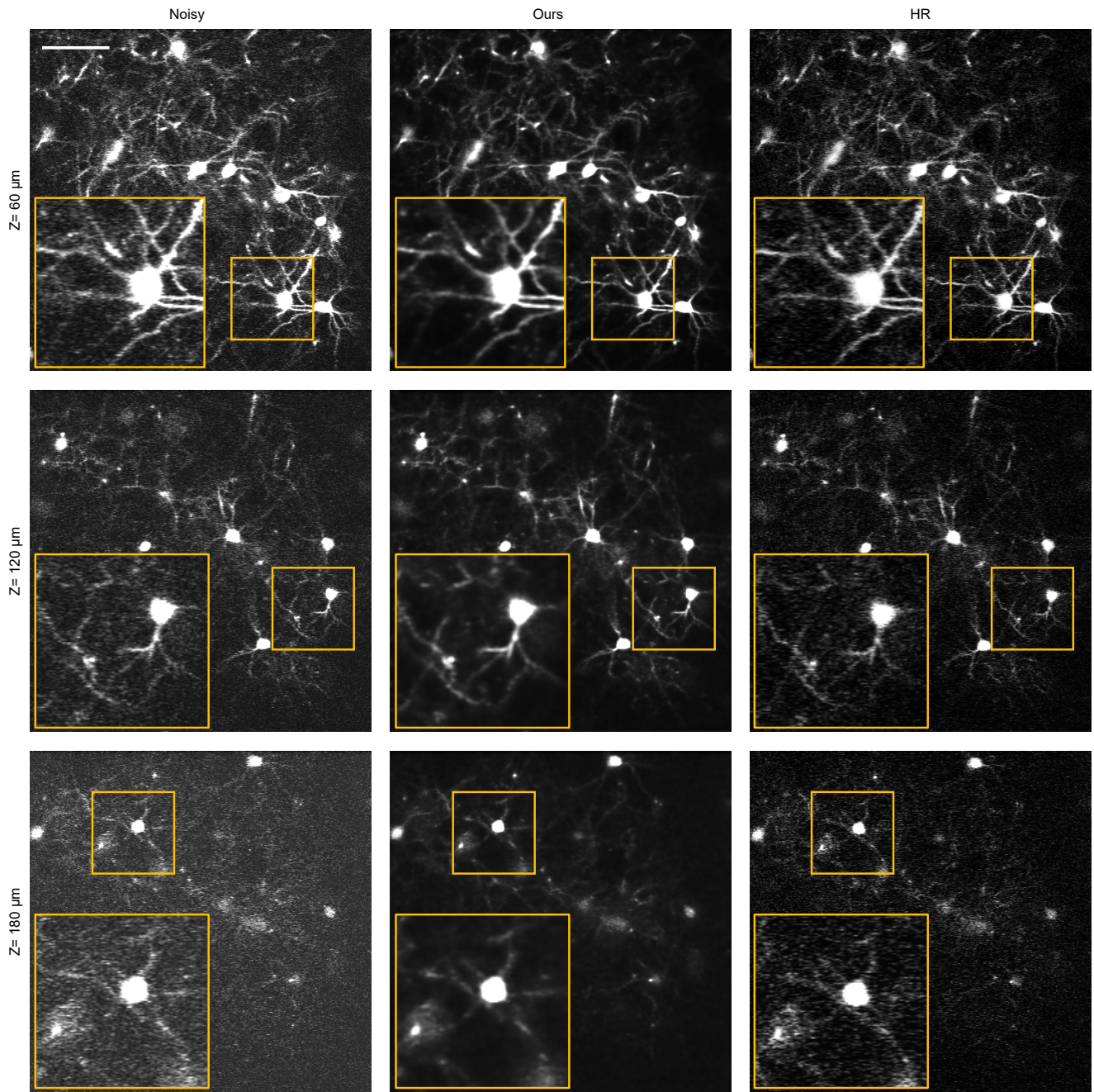
19

Supplementary Fig. S3. Max projection images for method comparison. A, Max projection images along y axis of the whole volume with $250 \times 250 \times 100 \mu\text{m}^3$ (200 planes, $0.5 \mu\text{m}/\text{pixel}$ in three axes), for comparison of different methods. Scale bar, $50 \mu\text{m}$. Magnified views of yellow-boxed regions are shown at the right of each image. B, Max projection images along x axis of the whole volume with $250 \times 250 \times 100 \mu\text{m}^3$ (200 planes, $0.5 \mu\text{m}/\text{pixel}$ in three axes), for comparison of different methods. Scale bar, $50 \mu\text{m}$. Magnified views of yellow-boxed regions are shown at the left of each image.



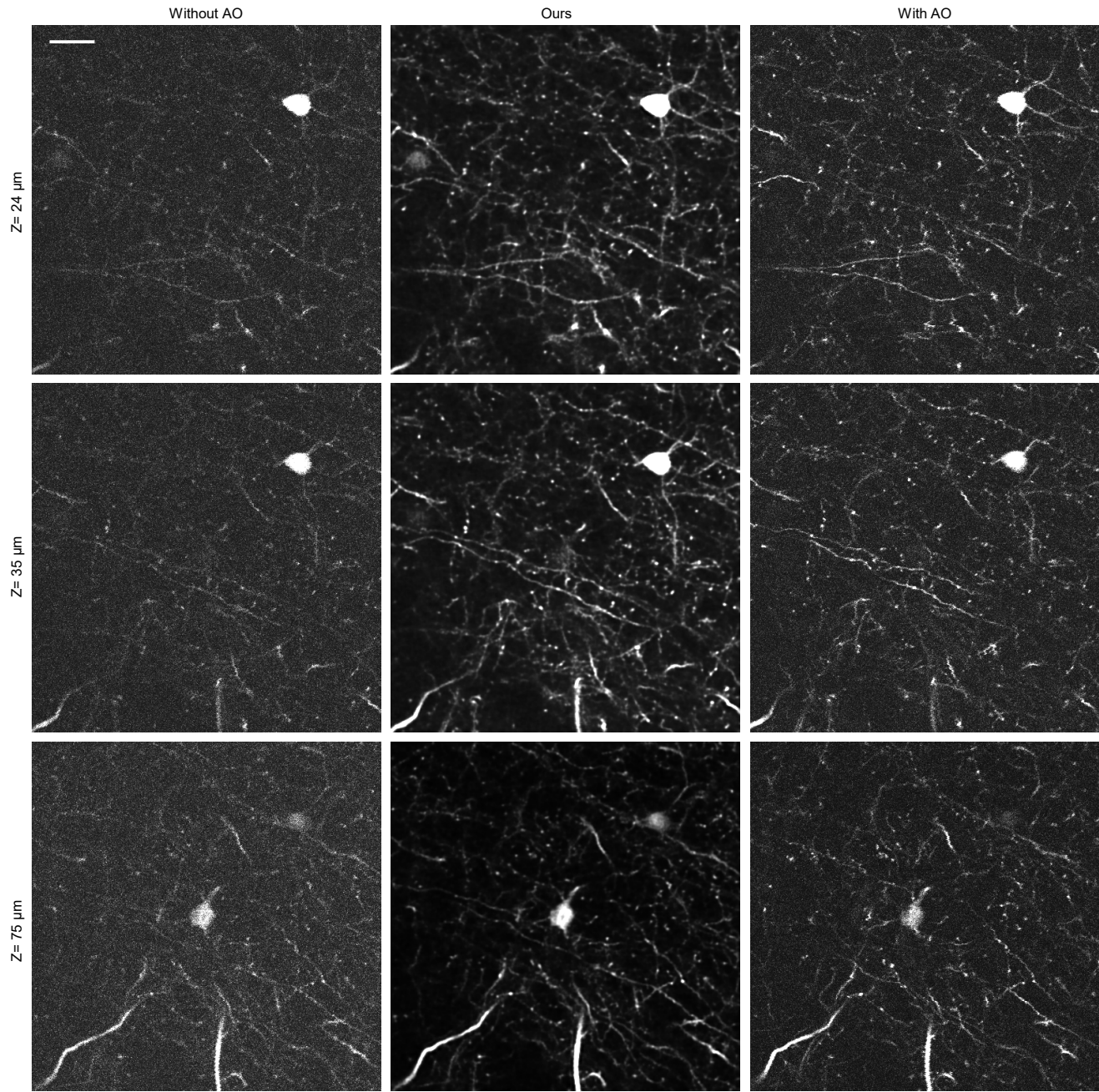
20

Supplementary Fig. S4. Denoising experimentally single neuron data with synchronized high-SNR reference. A, Representative max projections along z axis before and after denoising, which were used for pixel traces in Fig. 3D. 20 xy slices for this projection. Scale bar, 50 μm . Magnified views of yellow-boxed regions are shown at the left of each image. B, Representative max projections along y axis before and after denoising, which were used for pixel traces in Fig. 3E. 200 xz slices for this projection. Scale bar, 50 μm . Magnified views of yellow-boxed regions are shown at the left of each image. C, Representative max projections along x axis before and after denoising, which were used for pixel traces in Fig. 3E. 100 xy slices for this projection. Scale bar, 50 μm . Magnified views of yellow-boxed regions are shown at the right of each image.



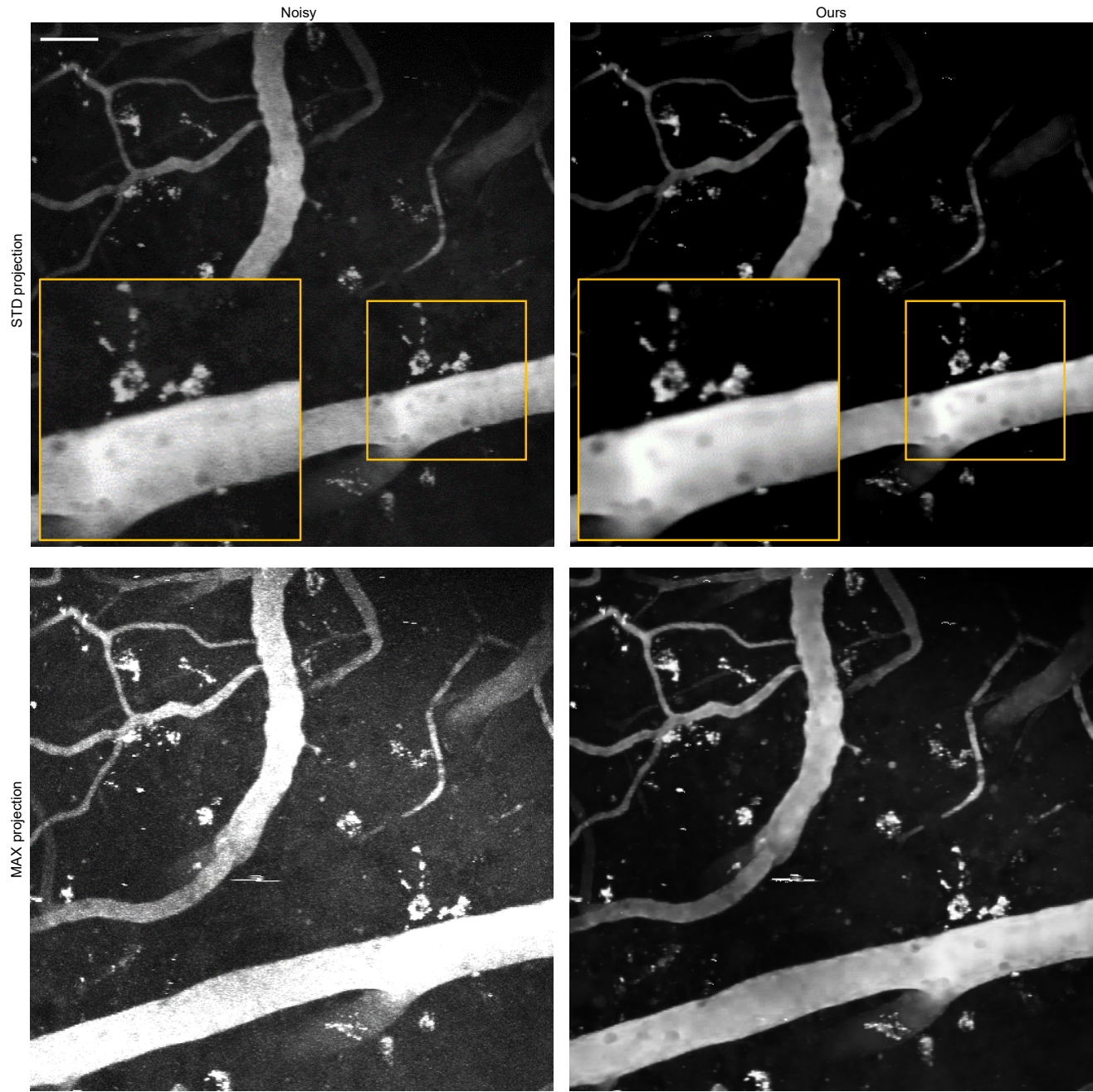
21

Supplementary Fig. S5. Denoising experimentally neuronal population data with synchronized high-SNR reference. Two-photon volumetric imaging neuronal population data were used to train our method, and high-SNR data were used as a reference. Three slices at different depths are represented here and each row shows one slice. Scale bar, $50 \mu m$. Magnified views of yellow-boxed regions are shown at the left bottom of each image.



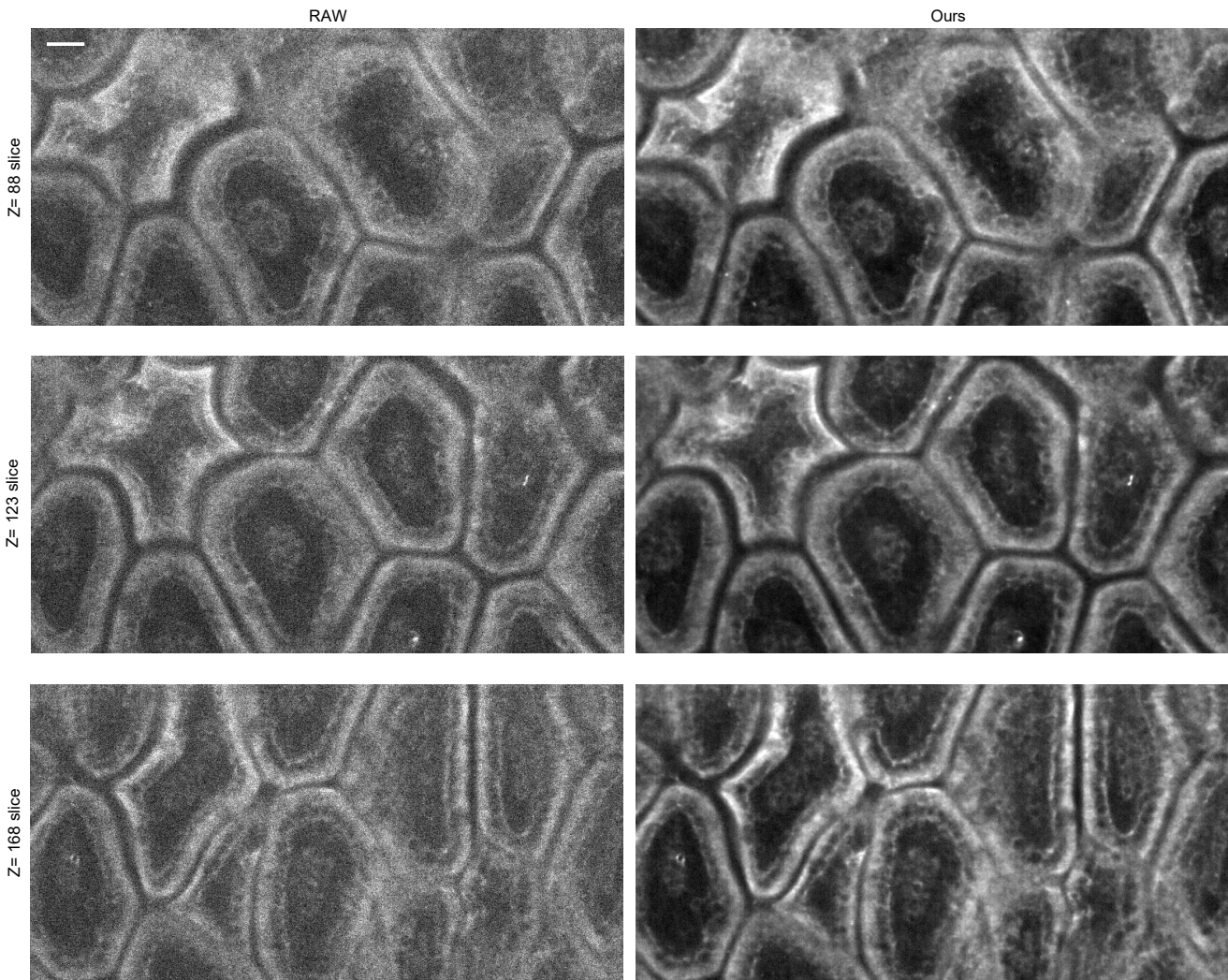
22

Supplementary Fig. S6. Denoising structural imaging data of dendrite and spine with synchronized high-SNR reference. Two-photon without AO imaging data of dendrite and spine were used to train our method, with AO data used as a reference. Three slices at different depths are represented here and each row shows one slice. Scale bar, 25 μm .



23

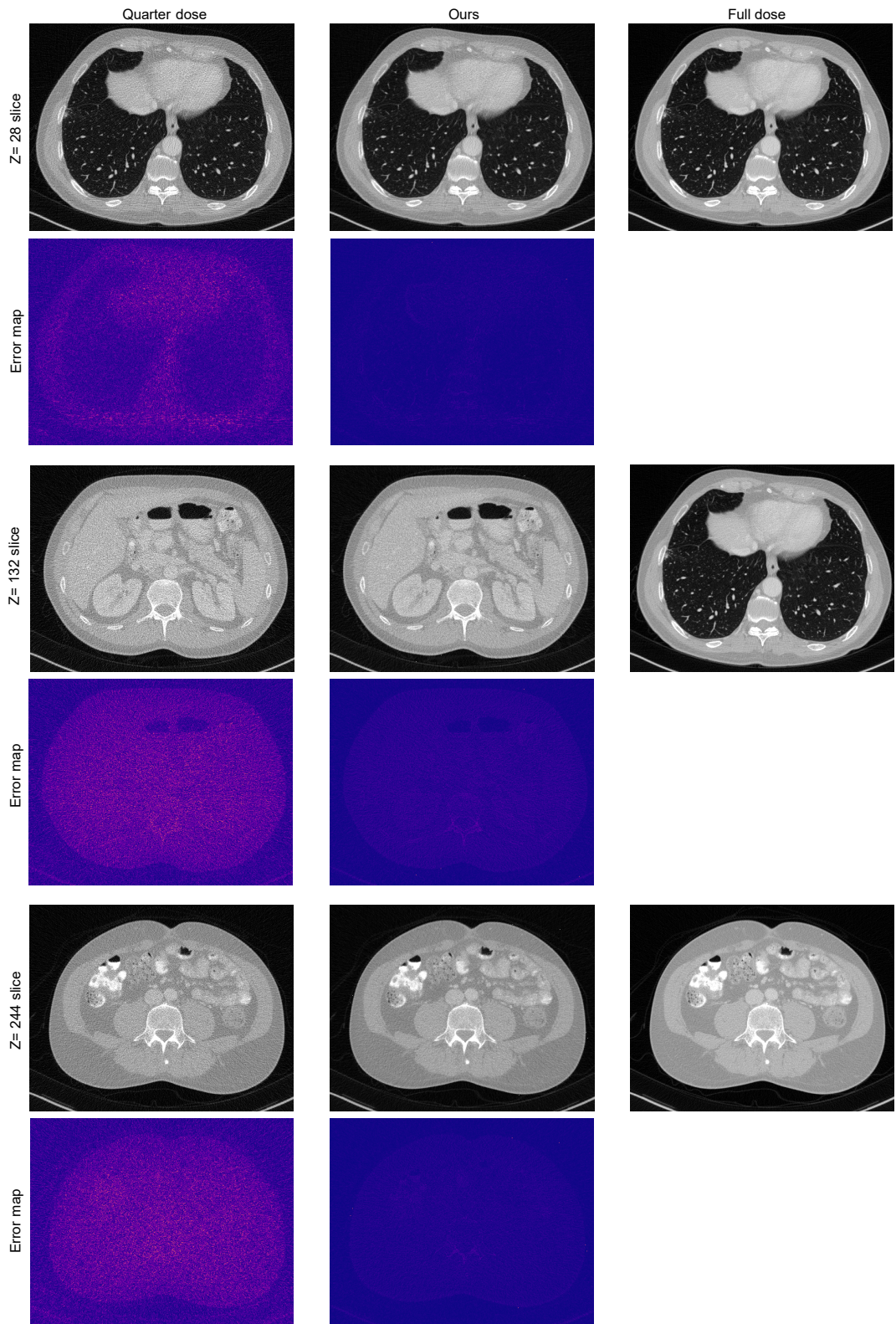
Supplementary Fig. S7. Applying SelfMirror on two-photon imaging of vessel sample. STD projection (top) and Max projection (bottom) of vessel data of a mouse cortex with a $250 \times 250 \times 100 \mu\text{m}^3$ volume. Left, raw data. Right, corresponding images using SelfMirror. Scale bars, $30 \mu\text{m}$. Magnified views of yellow-boxed regions are shown at the left bottom of each image.



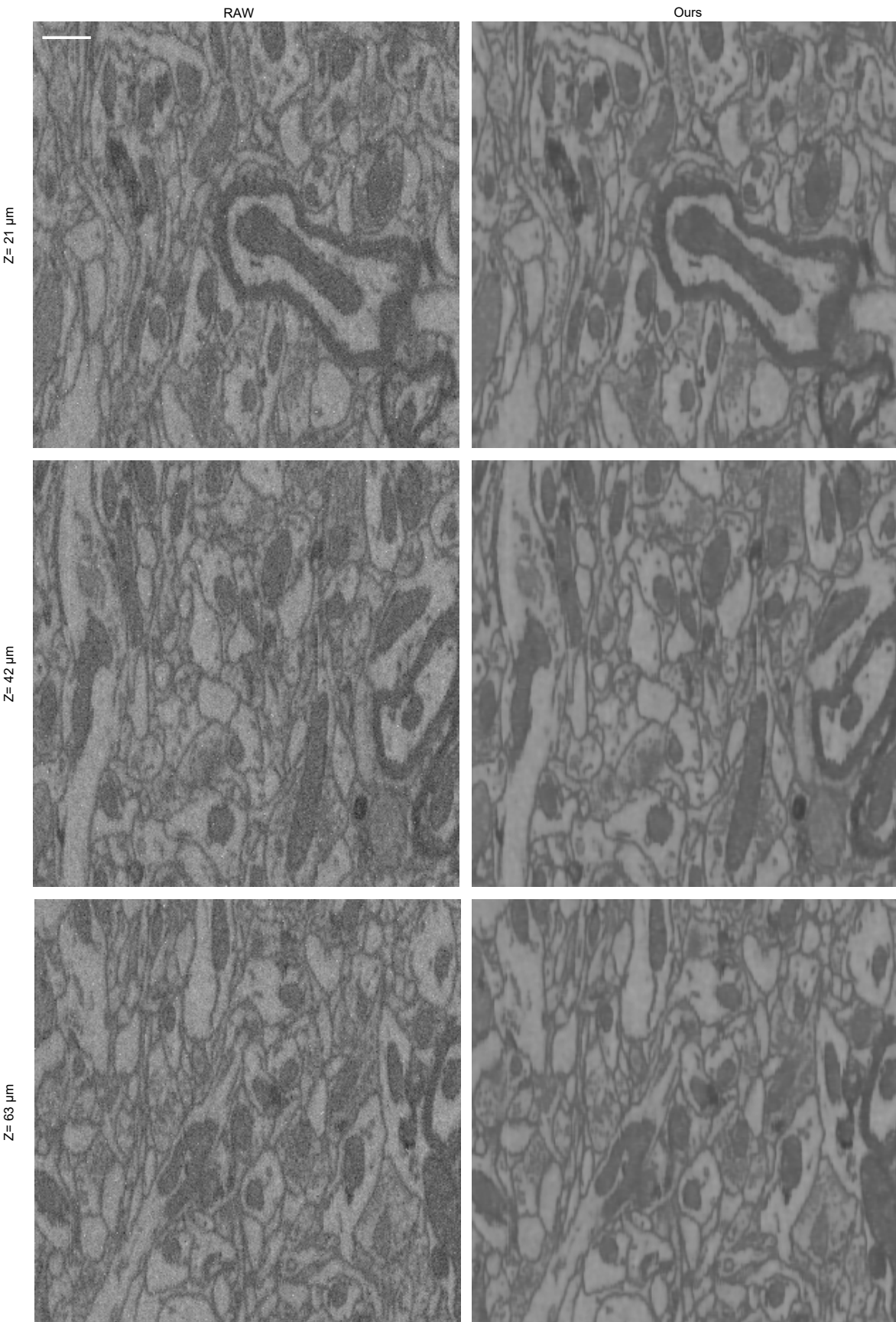
24

Supplementary Fig. S8. Applying SelfMirror on intestine of a mouse embryo after expansion.

Light sheet microscopy imaging data of the intestine of a mouse embryo after expansion. Three slices at different depths are represented here and each row shows one slice. Scale bar, $30 \mu m$.



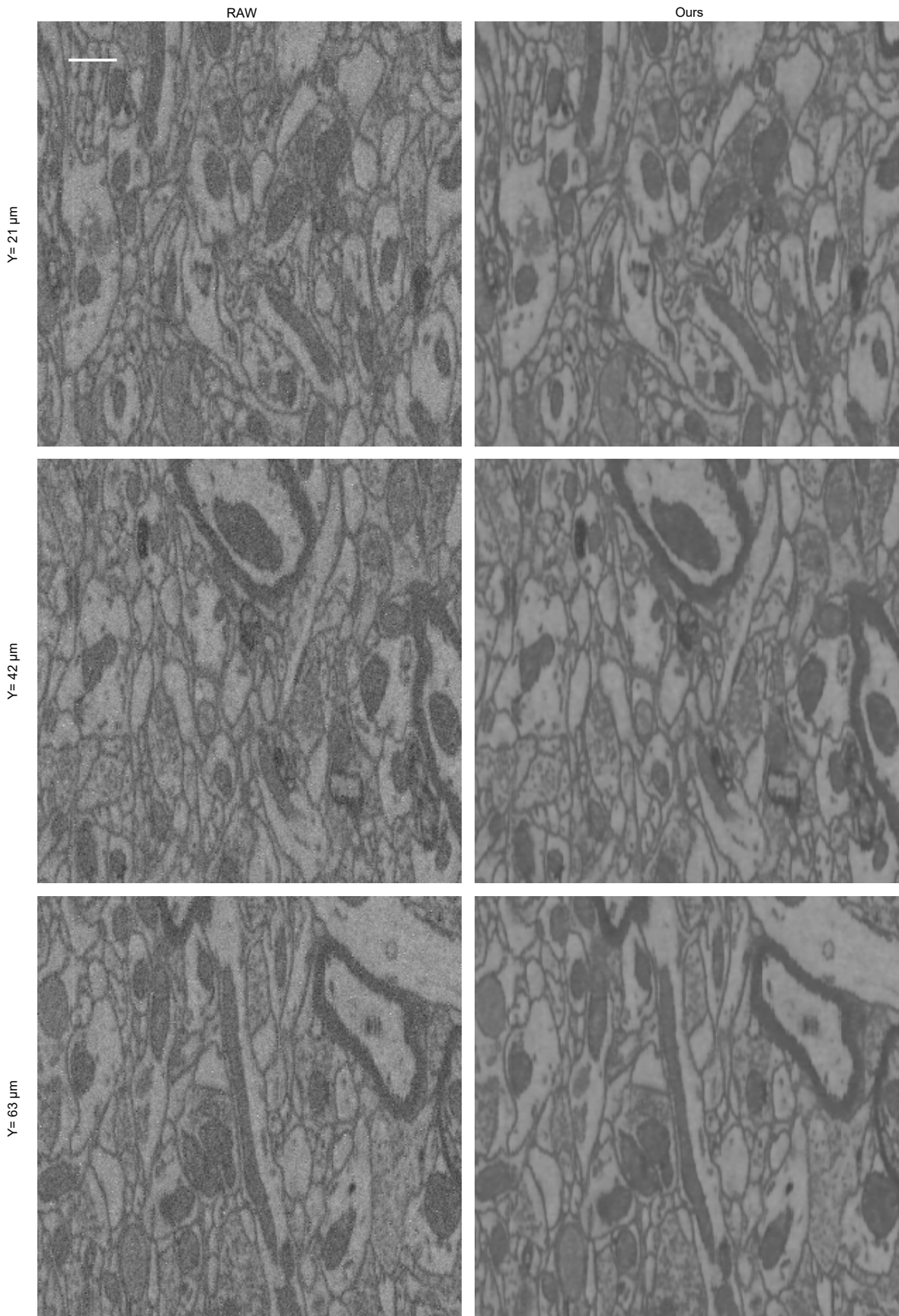
Supplementary Fig. S9. Applying SelfMirror on CT of a male's pleuroperitoneal cavity. CT data of the intestine of a male's pleuroperitoneal cavity. Three slices at different depths are represented here and each row shows one slice and the corresponding error map below the slice. Full dose CT data were used as the high-SNR reference. Left, quarter dose low-SNR images. Middle, SelfMirror denoising images. Right, full dose high-SNR images.



Supplementary Fig. S10. Applying SelfMirror on SEM data of a mouse somatosensory cortex

layer 4. SEM data of a mouse somatosensory cortex layer 4 with a $93 \times 60 \times 93 \mu m^3$. Left, raw data.

Right, corresponding images using SelfMirror. Three slices at different z depths are represented here and each row shows one slice. Scale bar, $10 \mu m$.



Supplementary Fig. S11. Applying SelfMirror on SEM data of a mouse somatosensory cortex

layer 4 . SEM data of a mouse somatosensory cortex layer 4 with a $93 \times 60 \times 93 \mu\text{m}^3$. Left, raw data.

Right, corresponding images using SelfMirror. Three slices at different depths along y axis are represented here and each row shows one slice. Scale bar, $10 \mu\text{m}$.

²⁸ **Supplementary Tables**

²⁹ **Supplementary Table S1:** Comparison of PSNR (upper table) and Pearson correlation coefficient (bottom
³⁰ table) along z axis of the whole volume.

³¹ **Supplementary Table S2:** Comparison of PSNR (upper table) and Pearson correlation coefficient (bottom
³² table) along y axis of the whole volume.

³³ **Supplementary Table S3:** Comparison of PSNR (upper table) and Pearson correlation coefficient (bottom
³⁴ table) along x axis of the whole volume.

³⁵

36 **Supplementary Videos**

37 **Supplementary Video S1. Simulated volumetric structural imaging of neurons**

38 **Supplementary Video S2. Two-photon volumetric imaging of single neurons in mouse**
39 **cortex.**

40 **Supplementary Video S3. Two-photon volumetric imaging of neuronal population in**
41 **mouse cortex.**

42 **Supplementary Video S4. Two-photon volumetric imaging of neuronal dendrites of mouse.**

43 **Supplementary Video S5. Confocal microscopy volumetric structural imaging of penicillin.**

44 **Supplementary Video S6. Two-photon volumetric imaging of cerebrovasculature of**
45 **mouse.**

46 **Supplementary Video S7. Expansion microscopy volumetric structural imaging of the**
47 **intestine of mouse embryos.**

48 **Supplementary Video S8. Computed tomography of human thoracoabdominal body.**

49 **Supplementary Video S9. Scanning electron microscopy volumetric imaging of cells from**
50 **mouse cortex.**

51 **References**

- 52 1. Song, A., Gauthier, J. L., Pillow, J. W., Tank, D. W. & Charles, A. S. Neural anatomy and optical
53 microscopy (naomi) simulation for evaluating calcium imaging methods. *J. neuroscience methods* **358**,
54 109173 (2021).

Supplementary Table S1. Comparison of PSNR (upper table) and Pearson correlation coefficient (bottom table) along z axis of the whole volume.

	RAW						DIP						N2F						N2S						N2V						Nc2Ne						SUPPORT						SelfMirror					
	Mean	SD	N	Mean	SD	N	Mean	SD	N	Mean	SD	N	Mean	SD	N	Mean	SD	N	Mean	SD	N	Mean	SD	N	Mean	SD	N	Mean	SD	N	Mean	SD	N															
P1	10.9506	0.329692	200	16.886438	0.674965	200	19.76731	0.351072	200	19.79267	0.333882	200	19.77317	0.345052	200	19.54785	0.351222	200	25.60665	5.04949	200	26.3452	1.772319	200																								
P2	13.42975	0.328997	200	17.6801	0.507668	200	20.1176	0.345384	200	20.07213	0.34231	200	19.99336	0.346636	200	19.73585	0.340103	200	24.09893	4.029423	200	23.25771	1.040399	200																								
P4	15.53226	0.3347	200	18.14332	0.441793	200	20.37607	0.348057	200	20.27257	0.337762	200	20.2147	0.348532	200	19.97416	0.350955	200	21.17433	2.097878	200	23.96889	0.686869	200																								
P8	17.15763	0.340737	200	18.35665	0.406074	200	20.56458	0.352618	200	20.56707	0.348242	200	20.33596	0.351813	200	20.14088	0.350261	200	20.16213	1.417605	200	20.98948	0.357257	200																								
P16	18.27186	0.346823	200	18.48599	0.416252	200	20.69206	0.351438	200	20.57866	0.352811	200	20.45562	0.351428	200	20.28178	0.351511	200	20.21791	1.427925	200	21.13754	0.356504	200																								
P32	18.96115	0.352923	200	18.54925	0.402634	200	20.76713	0.355287	200	20.64993	0.346722	200	20.52863	0.352615	200	20.33703	0.346641	200	20.20453	1.402886	200	21.14215	0.359868	200																								
P64	21.15832	0.353373	200	19.5779	0.449453	200	22.60849	0.351796	200	22.06577	0.334395	200	22.27114	0.354982	200	22.15809	0.344414	200	21.68584	1.78052	200	22.83236	0.364585	200																								
P128	26.94544	0.349095	200	21.43815	0.604669	200	27.68983	0.367992	200	27.1814	0.385181	200	26.61965	0.41204	200	27.73323	0.356123	200	25.61653	3.328069	200	27.74839	0.426951	200																								
	RAW						DIP						N2F						N2S						N2V						Nc2Ne						SUPPORT						SelfMirror					
	Mean	SD	N	Mean	SD	N	Mean	SD	N	Mean	SD	N	Mean	SD	N	Mean	SD	N	Mean	SD	N	Mean	SD	N	Mean	SD	N	Mean	SD	N	Mean	SD	N															
P1	0.295594	0.029067	200	0.393787	0.084345	200	0.848588	0.030417	200	0.816502	0.03296	200	0.830607	0.030348	200	0.802268	0.034319	200	0.639165	0.4197	200	0.89505	0.02059	200																								
P2	0.395326	0.035559	200	0.460873	0.081308	200	0.90191	0.018768	200	0.881226	0.020384	200	0.870979	0.022335	200	0.840378	0.028121	200	0.647657	0.425214	200	0.893879	0.013692	200																								
P4	0.507774	0.040733	200	0.50907	0.079117	200	0.935558	0.011327	200	0.906062	0.015988	200	0.899629	0.017628	200	0.859993	0.024868	200	0.660651	0.433672	200	0.924884	0.011551	200																								
P8	0.61674	0.041785	200	0.530623	0.076451	200	0.952343	0.008763	200	0.917959	0.013791	200	0.913186	0.016067	200	0.896094	0.018094	200	0.666861	0.437724	200	0.954647	0.009856	200																								
P16	0.704773	0.039744	200	0.540943	0.07663	200	0.960382	0.006829	200	0.93234	0.011458	200	0.922095	0.014772	200	0.903458	0.017284	200	0.670247	0.439934	200	0.958125	0.009128	200																								
P32	0.765025	0.036185	200	0.544957	0.07561	200	0.964321	0.006386	200	0.934117	0.011272	200	0.925945	0.014299	200	0.909957	0.016229	200	0.672362	0.441315	200	0.960717	0.008956	200																								
P64	0.8488	0.027611	200	0.550273	0.074021	200	0.967209	0.006069	200	0.949223	0.008929	200	0.93194	0.013409	200	0.924695	0.01325	200	0.673502	0.44206	200	0.9613	0.009083	200																								
P128	0.949158	0.010695	200	0.550833	0.072841	200	0.969127	0.005847	200	0.951626	0.009055	200	0.931917	0.013416	200	0.970923	0.004724	200	0.674436	0.442672	200	0.963495	0.00862	200																								

Supplementary Table S2. Comparison of PSNR (upper table) and Pearson correlation coefficient (bottom table) along y axis of the whole volume.

	RAW						DIP						N2F						N2S						N2V						Nc2Ne						SUPPORT						SelfMirror					
	Mean	SD	N	Mean	SD	N	Mean	SD	N	Mean	SD	N																																				
P1	10.32101	0.934145	500	16.24151	0.926417	500	19.14149	0.934444	500	19.17017	0.937207	500	19.14969	0.930377	500	18.93	0.941523	500	21.92783	0.978561	500	25.58116	1.512296	500																								
P2	12.79951	0.945007	500	17.0822	0.922609	500	19.4886	0.962122	500	19.44449	0.947736	500	19.36716	0.948433	500	19.11585	0.940751	500	21.50262	0.944375	500	22.69603	1.36992	500																								
P4	14.90108	0.965481	500	17.55503	0.920335	500	19.7451	0.983899	500	19.64672	0.936124	500	19.58679	0.962646	500	19.35004	0.965319	500	20.04626	0.907677	500	23.38591	1.071918	500																								
P8	16.52548	0.985549	500	17.77565	0.929232	500	19.9329	0.996024	500	19.9434	0.974489	500	19.70733	0.973428	500	19.5151	0.97441	500	19.32636	0.91193	500	20.35772	1.003116	500																								
P16	17.6391	1.008054	500	17.90578	0.930581	500	20.06004	1.002289	500	19.94813	0.997295	500	19.82641	0.978062	500	19.65555	0.978833	500	19.37846	0.916929	500	20.50582	1.001502	500																								
P32	18.3281	1.025725	500	17.97192	0.932977	500	20.13497	1.007344	500	20.02291	0.98049	500	19.89921	0.981132	500	19.71086	0.977534	500	19.37367	0.917767	500	20.51018	1.010107	500																								
P64	20.52523	1.028133	500	19.03468	0.993506	500	21.97731	0.993757	500	21.44184	0.897739	500	21.64553	0.963814	500	21.5324	0.944355	500	20.73046	0.940709	500	22.20173	0.998294	500																								
P128	26.31261	1.010759	500	21.02446	1.296226	500	27.07574	0.94168	500	26.58353	0.957497	500	26.04194	0.984942	500	27.1174	0.915553	500	23.85145	1.394786	500	27.13914	0.977538	500																								

	RAW						DIP						N2F						N2S						N2V						Nc2Ne						SUPPORT						SelfMirror					
	Mean	SD	N	Mean	SD	N	Mean	SD	N	Mean	SD	N	Mean	SD	N																																	
P1	0.284942	0.065292	500	0.358643	0.133556	500	0.831668	0.062325	500	0.790498	0.088551	500	0.810127	0.072301	500	18.93	0.941523	500	0.629773	0.133195	500	0.885394	0.032643	500																								
P2	0.38079	0.080953	500	0.423605	0.146647	500	0.891554	0.041284	500	0.866336	0.054759	500	0.856864	0.052576	500	19.11585	0.940751	500	0.679787	0.124605	500	0.892459	0.021074	500																								
P4	0.488596	0.094619	500	0.470112	0.152368	500	0.929097	0.026445	500	0.895193	0.044728	500	0.889192	0.040382	500	19.35004	0.965319	500	0.748278	0.106735	500	0.921985	0.019307	500																								
P8	0.593612	0.101065	500	0.492322	0.153608	500	0.947823	0.020844	500	0.909047	0.03952	500	0.90396	0.035983	500	19.5151	0.97441	500	0.768447	0.103224	500	0.94952	0.019614	500																								
P16	0.679557	0.100351	500	0.502813	0.153839	500	0.956528	0.017396	500	0.924352	0.066908	500	0.913764	0.032979	500	19.65555	0.978833	500	0.772912	0.102446	500	0.953297	0.018588	500																								
P32	0.739248	0.095872	500	0.50714	0.153898	500	0.960723	0.016128	500	0.928904	0.026612	500	0.917836	0.031832	500	19.71086	0.977534	500	0.775976	0.102083	500	0.956005	0.018217	500																								
P64	0.825253	0.079753	500	0.51299	0.153746	500	0.963843	0.014967	500	0.944443	0.024674	500	0.924582	0.029429	500	21.53524	0.944355	500	0.777699	0.101934	500	0.956448	0.018395	500																								
P128	0.936894	0.037787	500	0.513167	0.154266	500	0.965991	0.013702	500	0.945092	0.047788	500	0.924563	0.029532	500	27.1174	0.915553	500	0.77907	0.101733	500	0.95893	0.017504	500																								

Supplementary Table S3. Comparison of PSNR (upper table) and Pearson correlation coefficient (bottom table) along x axis of the whole volume.

	RAW						DIP						N2F						N2S						N2V						Nc2Ne						SUPPORT						SelfMirror					
	Mean	SD	N	Mean	SD	N	Mean	SD	N	Mean	SD	N	Mean	SD	N	Mean	SD	N	Mean	SD	N	Mean	SD	N	Mean	SD	N	Mean	SD	N	Mean	SD	N															
P1	10.25975	1.022834	500	16.18374	0.844436	500	19.08058	0.983091	500	19.11513	0.995716	500	19.08871	0.967691	500	18.87007	0.964777	500	21.88169	0.990594	500	25.55297	1.253987	500																								
P2	12.73801	1.037878	500	17.0244	0.85314	500	19.42702	1.024647	500	19.38316	1.007887	500	19.30575	0.994715	500	19.05592	0.972808	500	21.45264	0.963136	500	22.66408	1.183316	500																								
P4	14.83927	1.056308	500	17.49947	0.860399	500	19.68322	1.054699	500	19.5949	1.034531	500	19.52498	1.015424	500	19.28918	1.015916	500	19.98998	0.962316	500	23.338	0.93223	500																								
P8	16.46357	1.082494	500	17.71867	0.864467	500	19.87084	1.076389	500	19.88226	1.043222	500	19.64527	1.028688	500	19.45366	1.026528	500	19.26826	0.975161	500	20.29534	1.08365	500																								
P16	17.57707	1.106002	500	17.84939	0.867651	500	19.99797	1.084983	500	19.89063	1.074447	500	19.76425	1.038442	500	19.59423	1.023017	500	19.32039	0.980958	500	20.44347	1.082296	500																								
P32	18.26601	1.126903	500	17.91607	0.867354	500	20.07288	1.090719	500	19.95782	1.047031	500	19.83705	1.041651	500	19.64935	1.034779	500	19.31564	0.982684	500	20.44776	1.092517	500																								
P64	20.46312	1.130246	500	18.98571	0.8972	500	21.91524	1.06724	500	21.38493	0.95944	500	21.58321	1.004038	500	21.47423	0.978505	500	20.67693	0.986787	500	22.13899	1.066935	500																								
P128	26.25054	1.111412	500	21.01816	1.269017	500	27.01424	0.933059	500	26.52144	0.902613	500	25.98159	0.879409	500	27.05693	0.926779	500	23.8339	1.413597	500	27.07204	0.938681	500																								
	RAW						DIP						N2F						N2S						N2V						Nc2Ne						SUPPORT						SelfMirror					
	Mean	SD	N	Mean	SD	N	Mean	SD	N	Mean	SD	N	Mean	SD	N	Mean	SD	N	Mean	SD	N	Mean	SD	N	Mean	SD	N	Mean	SD	N	Mean	SD	N	Mean	SD	N												
P1	0.281308	0.074978	500	0.349967	0.133185	500	0.825693	0.070759	500	0.781176	0.10045	500	19.08871	0.967691	500	0.770133	0.091638	500	0.619011	0.144328	500	0.881789	0.033895	500																								
P2	0.375759	0.094172	500	0.413488	0.147553	500	0.888086	0.044521	500	0.859791	0.06866	500	19.30575	0.994715	500	0.812754	0.07897	500	0.669599	0.133105	500	0.889012	0.022232	500																								
P4	0.481506	0.112335	500	0.459491	0.153216	500	0.926684	0.030225	500	0.889371	0.070735	500	19.52498	0.015424	500	0.832963	0.075898	500	0.743111	0.105869	500	0.91955	0.019663	500																								
P8	0.584763	0.122355	500	0.481117	0.154077	500	0.946111	0.023899	500	0.905222	0.044207	500	19.64527	1.028688	500	0.877984	0.052202	500	0.766375	0.098671	500	0.947165	0.021394	500																								
P16	0.669373	0.124351	500	0.491944	0.15352	500	0.955187	0.020334	500	0.921796	0.050449	500	19.76425	1.038442	500	0.888529	0.050636	500	0.771343	0.09787	500	0.951241	0.019813	500																								
P32	0.728239	0.121869	500	0.496256	0.153174	500	0.959615	0.01843	500	0.924256	0.040241	500	19.83705	1.041651	500	0.893764	0.046606	500	0.774476	0.097574	500	0.953942	0.019386	500																								
P64	0.8133747	0.107145	500	0.502337	0.152024	500	0.962873	0.016524	500	0.940757	0.060481	500	21.58321	1.004038	500	0.912326	0.035529	500	0.776521	0.097294	500	0.954497	0.01954	500																								
P128	0.928919	0.057951	500	0.502928	0.151989	500	0.965135	0.014574	500	0.943708	0.040476	500	25.98159	0.879409	500	0.9067529	0.010575	500	0.777981	0.097212	500	0.956838	0.018941	500																								